

# Soot Particle Agglomeration Inlet (SPAI) for Enabling Online Chemical Composition Measurement of Nanoparticles with the Aerosol Mass Spectrometer

Sampsa Martikainen<sup>1\*</sup>, Sanna Saarikoski<sup>2</sup>, Paxton Juuti<sup>1</sup>, Hilikka Timonen<sup>2</sup>, Jorma Keskinen<sup>1</sup>, Panu Karjalainen<sup>1</sup>

<sup>1</sup> Aerosol Physics Laboratory, Tampere University, Tampere, Finland

<sup>2</sup> Atmospheric Composition Research, Finnish Meteorological Institute, Helsinki, Finland

## ABSTRACT

Nanoparticles are a topic of interest because of their effects on human health and the climate, but the current options for evaluating their chemical composition—one of the key properties that determine the mechanisms of these effects—remain very limited and often require long collection times. For example, the Soot Particle Aerosol Mass Spectrometer (SP-AMS) is an instrument that measures the chemical properties of particles in real time, but sampling loss fixes its lower particle size limit at 50 nm, thus excluding nanoparticles. Hence, we developed the *Soot Particle Agglomeration Inlet* (SPAI), an addition to the SP-AMS that enables it to detect and analyze nanoparticles by attaching them to the surfaces of artificially generated soot particles. We characterized and optimized the soot generation and the soot–nanoparticle agglomeration via laboratory testing and then assessed the SPAI’s performance using silver nanoparticles as the test aerosol. The SPAI increased the SP-AMS’s capability to detect the silver nanoparticles by 35 times, demonstrating its potential in resolving issues related to analyzing the chemical composition of nanoparticles, either as an enhancement of the SP-AMS or as an addition to other sample pretreatment systems.

**Keywords:** Aerosol characterization, Nanoparticle, Chemical composition

## OPEN ACCESS

**Received:** November 20, 2020

**Revised:** February 15, 2021

**Accepted:** February 16, 2021

\* **Corresponding Author:**  
sampsamartikainen@tuni.fi

### Publisher:

Taiwan Association for Aerosol  
Research

ISSN: 1680-8584 print

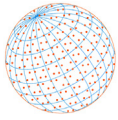
ISSN: 2071-1409 online

 **Copyright:** The Author's institution. This is an open access article distributed under the terms of the [Creative Commons Attribution License \(CC BY 4.0\)](https://creativecommons.org/licenses/by/4.0/), which permits unrestricted use, distribution, and reproduction in any medium, provided the original author and source are cited.

## 1 INTRODUCTION

High concentrations of nanoparticles (< 50 nm) are found in the atmosphere. In urban areas, they originate especially from anthropogenic sources such as traffic and small-scale combustion. Nanoparticles can have direct effects on human health and climate: The smallest nanoparticles have a high deposition efficiency in the respiratory system, and they can also translocate to other parts of the body, such as the brain (Oberdörster *et al.*, 2004; Maher *et al.*, 2016). Atmospheric aerosols affect the earth’s radiative forcing budget and thus climate in multiple different ways: directly through absorption/scattering of radiation and indirectly through impacts on cloud properties (Forster *et al.*, 2007). Many of these properties are affected by the chemical composition of the particles.

The chemical composition of aerosol particles is typically studied with offline methods, by collecting material on a filter or on an impactor plate and analyzing the particle mass collected. Lately, online methods have become more common. An example is the Soot Particle Aerosol Mass Spectrometer (SP-AMS; Aerodyne Research, Inc.), that can be used both for non-refractory substances that evaporate at the tungsten vaporizer operated at 600°C, as well as for absorbing refractory components at about 4000°C. The latter is made possible by the soot particle (SP) module developed as an addition to the original AMS system (Onasch *et al.*, 2012) and is typically



used to quantify the amount of the refractory black carbon (rBC) in the aerosol.

Due to particle losses in the aerodynamic lens system in the inlet of the SP-AMS, the transmission efficiency of particles smaller than 50 nm or larger than 1  $\mu\text{m}$  (vacuum aerodynamic diameter) is poor (Liu *et al.*, 2007), meaning that a major fraction of nanoparticles is left out of reach. With the SP module also comes a challenge of overlapping the particle and laser beams: The collection efficiencies of both rBC and the particle matter associated with it are strongly influenced by the overlap. The overlap in turn is affected by particle properties, as the divergence from the center of the particle beam depends on the particle size, morphology and chemical composition (Liu *et al.*, 1995; Huffman *et al.*, 2005; Willis *et al.*, 2014). Particles that neither absorb the wavelength of the laser (1064 nm) nor evaporate at 600°C cannot be detected by the instrument.

The options for measuring the chemical composition of nanoparticles online are very limited. Combining a Scanning Mobility Particle Sizer (SMPS; TSI Inc.) and inductively coupled plasma mass spectrometry (ICP-MS) has been presented (Hess *et al.*, 2015). The drawbacks of this system are high cost and low portability. Single-particle mass spectrometry (SPMS) can be used to analyze the chemical composition and size of single particles in near-real time. Examples of such instruments are Aerosol Time-of-Flight Mass Spectrometer (AToFMS; Prather *et al.*, 1994) and Single-Particle Laser Ablation Time-of-Flight Mass Spectrometer (SPLAT-MS; Zelenyuk and Imre, 2005). These techniques suffer from particle losses before the detection part of the instrument as well, and they are limited by their non-quantitative nature. There is a fundamental need for a system that could be applied in all sorts of measurement environments to study the detailed nanoparticle composition online.

In this study we present a measurement concept and a prototype system enabling the measurement of chemical composition of nanoparticles online. In the concept, the studied nanoparticles are attached on the surfaces of artificially generated soot particles. We call this soot particle generation and agglomeration process the *Soot Particle Agglomeration Inlet* (SPAI). The system is designed as an inlet to the SP-AMS. We applied the prototype in laboratory tests, where the soot particle generation and the agglomeration section were characterized and optimized, and the performance of the SPAI was evaluated with silver nanoparticles as test aerosol.

## 2 THE CONCEPT OF THE SPAI

The concept of the SPAI is illustrated in Fig. 1. The unknown aerosol is mixed with soot particles and led to an agglomeration chamber, a large volume compared to the sample line, resulting in a long residence time. The studied particles then coagulate with the soot particles. The sample flow is created with an ejector diluter (ED), after which the mixture is led to the SP-AMS. The desired test and soot aerosol flows are set by constricting the lines with adjustable valves. In the prototype system, the soot particles are generated by burning acetylene ( $\text{C}_2\text{H}_2$ ) with a flat flame burner (McKenna Products) under fuel-rich conditions, but any device capable of producing a suitable soot mode is a viable option. The combustion products are treated with a catalytic stripper (CS; Amanatidis *et al.*, 2018) operating at 350°C to remove volatile compounds, ideally leaving only the non-volatile fraction of soot.

Downstream the agglomeration chamber, ideally all the tested aerosol particles are attached to soot particles mainly larger than 50 nanometers in size and can thus penetrate the aerodynamic lens. Soot particles then reach the laser in the SP part, absorbing a great deal of energy. Heat is transferred from the high-temperature soot particles to the coating. Ideally, both the soot and coating are entirely evaporated, further ionized, and efficiently transferred to the detection part of the instrument.

## 3 METHODS

The test aerosol was created by producing silver particles with a tube furnace method (Scheibel and Porstendörfer, 1983), using nitrogen as carrier gas. Silver particles were chosen as the test aerosol for two main reasons. Firstly, silver has properties that we were looking for in the benchmarking tests: It is a non-volatile metal that does not evaporate in the vaporizer and it has two distinctive isotopes in the AMS high-resolution spectrum ( $m/z$  106.905 and 108.905). Secondly,

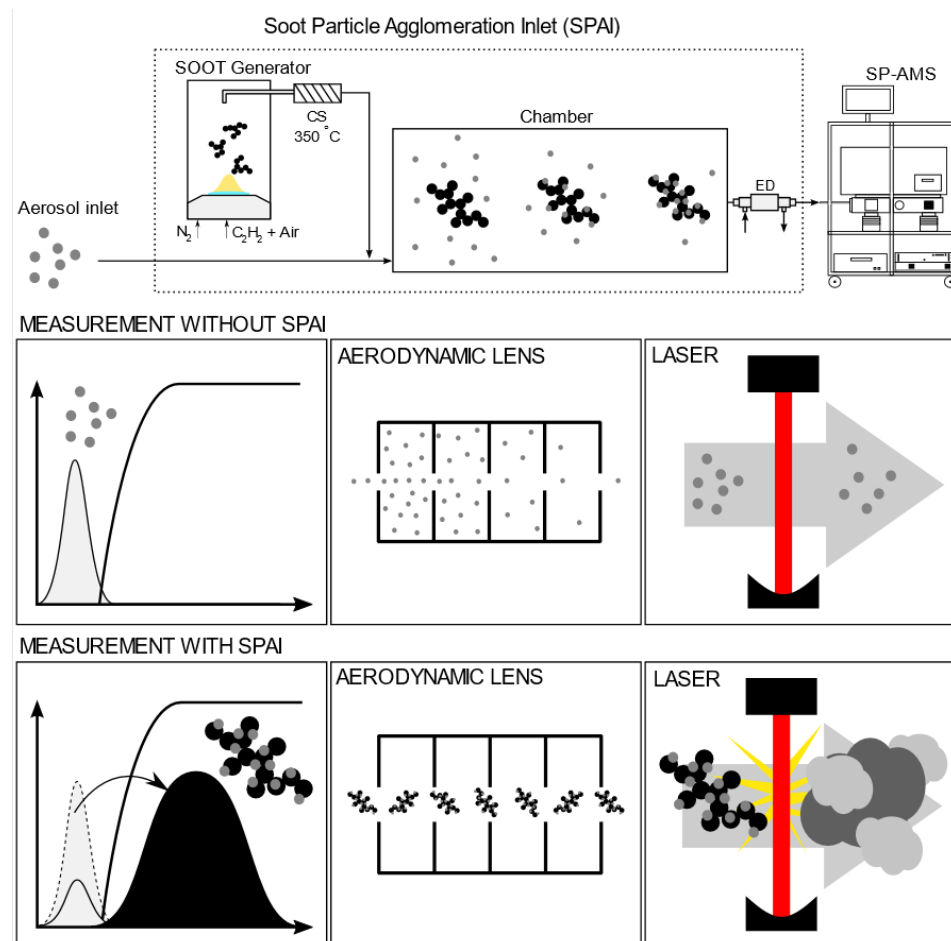
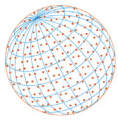


**Fig. 1.** The concept of the SPAI.

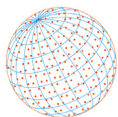
our laboratory infrastructure for generation of silver nanoparticles is well established and we are experienced in controlling, e.g., the size distributions of the particles. The SP-AMS has been shown to be sensitive to silver (and other metal) particles (Nilsson *et al.*, 2015). However, the addition of SPAI provides the advantages of (1) increased penetration of nanoparticles through the aerodynamic lens and (2) more efficient evaporation of the reflective elements, as they lie on the surfaces of soot particles that absorb the wavelength of the laser extremely well.

An SMPS operated with Model 3081 Differential Mobility Analyzer (DMA) was used to determine the particle size distribution. Particle densities at selected particle diameters (17.8 nm and 112 nm) were determined with a Combustion Centrifugal Particle Mass Analyzer (CPMA; Olfert and Collings, 2005) coupled with a DMA.

Adjusting the furnace temperature allowed for manipulation of the silver particle size distribution. Similarly, the soot particle properties were varied by adjusting fuel flow and thus the stoichiometric ratio of combustion. Prior to the measurements, both generation systems were tested to determine how the adjusted parameters affect the generated particles and to find a few distinctive soot and silver particle size distributions for the tests. The stabilities of the systems with the chosen parameter values were also verified. In the tests, a cylinder-shaped volume of approximately 7 L was used as the agglomeration chamber. With the inlet flow of the ED (4.7 L min<sup>-1</sup>), the residence time in the agglomeration section is estimated to be 90 seconds.

Three different silver modes were tested, corresponding to furnace temperatures of 1100°C, 1150°C and 1200°C. Similarly, three soot modes were generated, corresponding to burner fuel feeds of 0.9 L min<sup>-1</sup>, 0.92 L min<sup>-1</sup> and 0.95 L min<sup>-1</sup>. The modes are from now on referred to as “low,” “med” and “high,” referring to both the concentration of the generated substance (silver or soot) and the adjusted parameters (temperature or flow).

The measured silver modes extended below the lower size limit of the SMPS (6.85 nm). In



order to accurately estimate how much silver agglomerated with soot, modal fits for the measured size distributions were constructed by assuming a lognormal size distribution:

$$\frac{dN}{d\ln(D_p)} = \frac{N_{tot}}{\sqrt{2\pi} \ln(\sigma_g)} \exp\left(-\frac{(\ln(D_p) - \ln(D_g))^2}{2\ln^2(\sigma_g)}\right) \quad (1)$$

where  $N$  is the particle concentration,  $D_p$  particle diameter,  $N_{tot}$  total particle concentration,  $\sigma_g$  geometric standard deviation and  $D_g$  the geometric mean diameter. The appropriate values for these variables were found by least squares method, minimizing the error between the fit and measured values.

The SP-AMS is a mass-based instrument and in order to compare the concentrations measured by it and the SMPS, the number concentrations needed to be converted to mass concentrations. In order to achieve this, silver particle density as a function of particle diameter was needed. Silver particles generated with the tube furnace method form agglomerates (Scheibel and Porstendörfer, 1983; Ku and Maynard, 2006). Using the fractal dimension of the agglomerates, the effective density of particles can be described as:

$$\log(\rho_{eff}) = -(3 - fd) \log\left(\frac{D_{mob}}{D_{ref}}\right) + \log(\rho_{ref}) \quad (2)$$

where  $\rho_{eff}$  is the effective density,  $fd$  the fractal dimension,  $D_{mob}$  the mobility diameter and  $D_{ref}$  the upper particle diameter limit for particles with the reference density  $\rho_{ref}$  and spherical shape. The density of agglomerate-shaped particles has been successfully described with this method in previous studies (e.g., Ristimäki, 2006; Skillas *et al.*, 1998).

The effective density of silver particles was determined for two mobility diameters (17.8 nm and 112 nm, corresponding to densities of 6.11 g cm<sup>-3</sup> and 2.30 g cm<sup>-3</sup>, respectively). If the density of silver at room temperature (10.49 g cm<sup>-3</sup>) is assumed as the reference density  $\rho_{ref}$ , the remaining unknown variables  $fd$  and  $D_{ref}$  can be solved from Eq. (2), which yields 2.3035 nm and 6.1106 nm, respectively.

The validity of the density function was tested by the following method. First, the number size distribution of the generated silver particles was measured without the agglomeration chamber. It was then measured again after the agglomeration chamber, letting the particles grow due to agglomeration. Thus, two different size distributions with equal mass were obtained. After calculating the mass concentrations with and without the density correction and comparing the obtained results, it was found that assuming constant density resulted in almost 3-fold difference, whereas applying the density correction resulted in a difference less than 4%.

The particle diameters in the distributions measured with the SMPS are electrical mobility diameters, whereas the mentioned SP-AMS cutoff (~50 nm) is a vacuum aerodynamic diameter. In order to link the two, a relation presented by Jimenez *et al.* (2003) was used:

$$D_{va} = \frac{\rho_p D_v}{\rho_0 X_v} \quad (3)$$

where  $D_{va}$  is the vacuum aerodynamic diameter,  $D_v$  is the volume-equivalent diameter,  $X_v$  is the dynamic shape factor,  $\rho_p$  is the density of the particle material and  $\rho_0$  is unit density. For a spherical particle  $D_v = D_{mob}$  and  $X_v = 1$ . Thus, a spherical silver particle with a vacuum aerodynamic diameter of 50 nm has a mobility diameter of 4.8 nm. Since the upper diameter limit for spherical particles was determined to be 6.11 nm, the spherical shape assumption is valid.

The data obtained with the SP-AMS was analyzed with Igor Pro (v. 6.37) software, including packages Squirrel (v. 1.57) and Pika (v. 1.16). Collection efficiency (CE) and relative ionization efficiency (RIE) of 1 were used for the calculation of silver mass. Prior to the measurements, default calibrations with ammonium nitrate and REGAL black were performed. The main goal for the measurements was to generally test the functionality of the concept and thus no specific calibration for silver was performed.

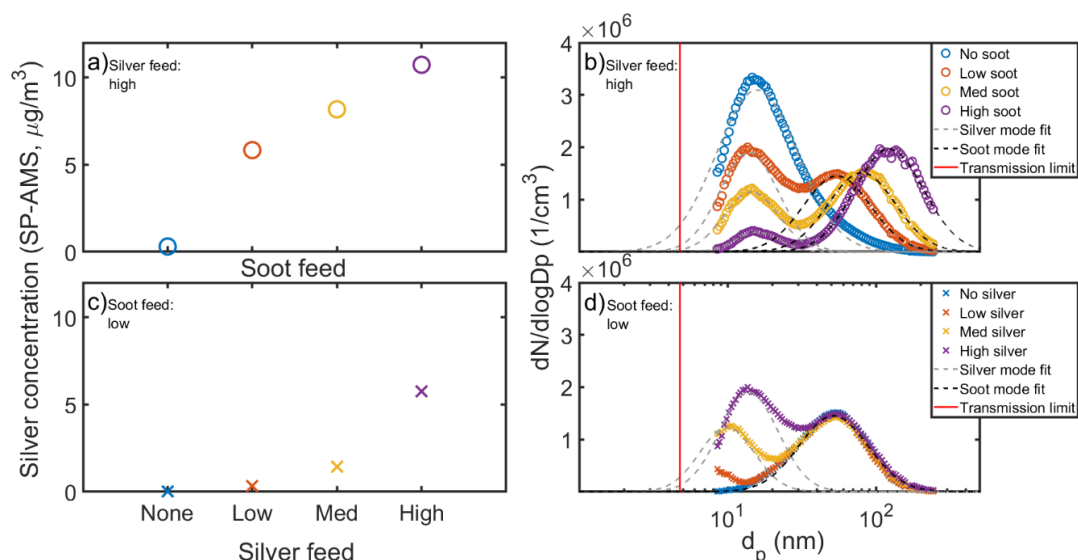
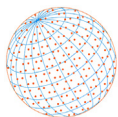


**Fig. 2.** Enhancement of elemental silver detection in the SP-AMS by the level of generated (a) soot and (c) silver and (b, d) corresponding particle size distributions from SMPS. Red line represents the vacuum aerodynamic diameter of 50 nm converted to electrical mobility, assuming the density of silver and spherical shape of particles.

## 4 RESULTS AND DISCUSSION

Results from the laboratory tests are shown in Fig. 2. The subfigures on the right side (b and d) contain the size distributions obtained while varying the soot or silver feed while keeping the other constant. Both the measured distributions and the modal fits are shown. The red line labeled as *Transmission limit* represents the vacuum aerodynamic diameter of 50 nm, converted to electrical mobility diameter (4.8 nm) as presented in the section “Methods.” In the left subfigures (a and c), the corresponding calculated elemental silver mass concentrations from the SP-AMS are shown. Note that one measurement point (high silver feed combined with low soot feed) is presented in both upper and lower subfigures. Further results obtained from the measured silver concentrations and particle size distributions are presented in Table 1.

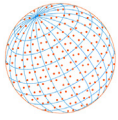
With constant soot feed (low), varying the silver feed increases the silver mass detected by SP-AMS ( $0.32 \mu\text{g m}^{-3}$ ,  $1.44 \mu\text{g m}^{-3}$  and  $5.75 \mu\text{g m}^{-3}$  for low, medium, and high silver feed, respectively), which is seen in Fig. 2(c). The agglomerated silver does not cause a visible change in the soot mode (Fig. 2(d)).

Larger soot modes scavenge more silver particles which can be seen from the size distributions in Fig. 2(b). The scavenged silver mass fractions are 0.80, 0.89 and 0.97 for low, medium, and high soot feeds, respectively. Changing the soot feed had a dramatic impact on the silver detected with the SP-AMS. Without soot, the measured concentration was  $0.3 \mu\text{g m}^{-3}$ . With low, medium, and high soot feed the detected silver concentrations were approximately  $6 \mu\text{g m}^{-3}$ ,  $8 \mu\text{g m}^{-3}$  and

**Table 1.** The effect of soot feed of SPAI on the silver agglomerated with soot (mass and number), agglomeration ratio (the fraction of silver agglomerated with soot), silver mass detected by SP-AMS, detection ratio of SP-AMS (the fraction of silver mass agglomerated with soot that is detected) and improvement in the silver detection of SP-AMS.

Soot feed	Silver agglomerated with soot		Agglomeration ratio		Silver mass <sup>1</sup> (SP-AMS, $\mu\text{g m}^{-3}$ )	SP-AMS detec. ratio <sup>1</sup>	Detec. improvement factor
	Mass ( $\mu\text{g m}^{-3}$ )	Number ( $10^6 \text{ cm}^{-3}$ )	Mass	Number			
None	-	-	-	-	0.30	-	-
Low	54.63	1.192	0.801	0.558	5.84	0.107	19.2
Med	60.47	1.606	0.887	0.752	8.18	0.135	26.9
High	66.07	1.997	0.969	0.935	10.73	0.162	35.4

<sup>1</sup> With default SP-AMS calibration.



11  $\mu\text{g m}^{-3}$ , respectively. In other words, applying the SPAI increased the silver detection by a factor of up to 35. Due to high density, even small (in terms of electrical mobility diameter) silver particles are able to penetrate the aerodynamic lens. The increased silver detection in the SP-AMS is thus mainly attributed to the enhancement in the evaporation (and consequently in the RIE) of silver in the SP-AMS.

Looking at the measurement points presented in Table 1, silver mass agglomerated with soot (estimated from the size distributions as presented in the section “Methods”) is 6–10 times higher than the silver mass detected by SP-AMS. This is explained partly by the instrument not being calibrated for silver and partly by silver simply not reaching the detection part of the instrument, due to agglomeration with suboptimal-sized soot particles.

## 5 CONCLUSIONS

Our initial results on the SPAI’s capability to detect nanoparticles for chemical analysis are promising. While we have tested this approach only with silver aerosol, it can theoretically be applied to any type of nanoparticles. However, it is best suited to species not found in the generated soot aerosol, e.g., metals.

Further research on the SPAI-enhanced SP-AMS should focus on calibrating it for different substances, identifying the optimal size distribution for the soot particles and developing the system for specific applications, e.g., investigating the chemical composition of < 23 nm particles exhausted by engines, for which we lack sufficient data. Ideally, the generated soot should achieve high penetration through the aerodynamic lens, exhibit high absorptivity at 1064 nm (the wavelength of the laser in the SP module), enable a high rate of agglomeration for the target particles and be free of any impurities that might interfere with the signals originating from the studied nanoparticles.

Finally, we can analyze a particular fraction of an aerosol by employing additional sample pretreatment systems. For example, the non-volatile content can be examined with a thermal denuder, catalytic stripper or aerosol–gas exchange system (Bainschab *et al.*, 2019), or particles in a size range can be selected by a pre-impactor, DMA, CPMA or differential diffusion analyzer (Arffman *et al.*, 2017). Furthermore, since nanoparticle mass concentrations tend to be low, an aerosol concentrator (Saarikoski *et al.*, 2019) could be used to further enhance the detection.

## ACKNOWLEDGMENTS

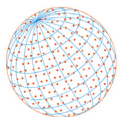
This work was conducted partly in DownToTen project, funded by the European Union’s Horizon 2020 research and innovation programme under Grant Agreement No. 724085. S.M. acknowledges funding from Kone Foundation, and P.K. acknowledges funding from Academy of Finland project EFFi Decision No. 322120.

## DISCLAIMER

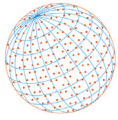
The authors declare that there is no conflict of interest.

## REFERENCES

- Amanatidis, S., Ntziachristos, L., Karjalainen, P., Saukko, E., Simonen, P., Kuittinen, N., Aakko-Saksa, P., Timonen, H., Rönkkö, T., Keskinen, J. (2018). Comparative performance of a thermal denuder and a catalytic stripper in sampling laboratory and marine exhaust aerosols. *Aerosol Sci. Technol.* 52, 420–432. <https://doi.org/10.1080/02786826.2017.1422236>
- Arffman, A., Juuti, P., Harra, J., Keskinen, J. (2017). Differential diffusion analyzer. *Aerosol Sci. Technol.* 51, 1429–1437. <https://doi.org/10.1080/02786826.2017.1367089>
- Bainschab, M., Martikainen, S., Keskinen, J., Bergmann, A., Karjalainen, P. (2019). Aerosol gas exchange system (AGES) for nanoparticle sampling at elevated temperatures: Modeling and experimental characterization. *Sci. Rep.* 9, 17149. <https://doi.org/10.1038/s41598-019-53113-5>



- Forster, P., Ramaswamy, V., Artaxo, P., Berntsen, T., Betts, R., Fahey, D.W., Haywood, J., Lean, J., Lowe, D.C., Myhre, G., Nganga, J., Prinn, R., Raga, G., Schulz, M., Van Dorland, R. (2007). Changes in Atmospheric Constituents and in Radiative Forcing. *Climate Change 2007: The Physical Science Basis*. in: Solomon, S., Qin, D., Manning, M., Chen, Z., Marquis, M., Averyt, K.B., Tignor, M., Miller, H.L. (Eds.), Contribution of Working Group I to the Fourth Assessment Report of the Intergovernmental Panel on Climate Change Cambridge University Press, Cambridge, United Kingdom and New York, NY, USA.
- Hess, A., Tarik, M., Ludwig, C. (2015). A hyphenated SMPS-ICPMS coupling setup: Size-resolved element specific analysis of airborne nanoparticles. *J. Aerosol Sci.* 88, 109–118. <https://doi.org/10.1016/j.jaerosci.2015.05.016>
- Huffman, J.A., Jayne, J.T., Drewnick, F., Aiken, A.C., Onasch, T., Worsnop, D.R., Jimenez, J.L. (2005). Design, modeling, optimization, and experimental tests of a particle beam width probe for the aerodyne aerosol mass spectrometer. *Aerosol Sci. Technol.* 39, 1143–1163. <https://doi.org/10.1080/02786820500423782>
- Jimenez, J.L., Bahreini, R., Cocker III, D.R., Zhuang, H., Varutbangkul, V., Flagan, R.C., Seinfeld, J.H., O’Dowd, C.D., Hoffmann, T. (2003). New particle formation from photooxidation of diiodomethane (CH<sub>2</sub>I<sub>2</sub>). *J. Geophys. Res.* 108, 4318. <https://doi.org/10.1029/2002JD002452>
- Ku, B.K., Maynard, A.D. (2006). Generation and investigation of airborne silver nanoparticles with specific size and morphology by homogeneous nucleation, coagulation and sintering. *J. Aerosol Sci.* 37, 452–470. <https://doi.org/10.1016/j.jaerosci.2005.05.003>
- Liu, P., Ziemann, P.J., Kittelson, D.B., McMurry, P.H. (1995). Generating particle beams of controlled dimensions and divergence: II. Experimental evaluation of particle motion in aerodynamic lenses and nozzle expansions. *Aerosol Sci. Technol.* 22, 314–324. <https://doi.org/10.1080/02786829408959749>
- Liu, P.S.K., Deng, R., Smith, K.A., Williams, L.R., Jayne, J.T., Canagaratna, M.R., Moore, K., Onasch, T.B., Worsnop, D.R., Deshler, T. (2007). Transmission efficiency of an aerodynamic focusing lens system: Comparison of model calculations and laboratory measurements for the Aerodyne Aerosol Mass Spectrometer. *Aerosol Sci. Technol.* 41, 721–733. <https://doi.org/10.1080/02786820701422278>
- Maher, B.A., Ahmed, I.A.M., Karloukovski, V., MacLaren, D.A., Foulds, P.G., Allsop, D., Mann, D.M.A., Torres-Jardón, R., Calderon-Garciduenas, L. (2016). Magnetite pollution nanoparticles in the human brain. *PNAS* 113, 10797–10801. <https://doi.org/10.1073/pnas.1605941113>
- Nilsson, P.T., Eriksson, A.C., Ludvigsson, L., Messing, M.E., Nordin, E.Z., Gudmundsson, A., Mueller, B.O., Deppert, K., Fortner, E.C., Onasch, T.B., Pagels, J.H. (2015). In-situ characterization of metal nanoparticles and their organic coatings using laser-vaporization aerosol mass spectrometry. *Nano Res.* 8, 3780–3795. <https://doi.org/10.1007/s12274-015-0877-9>
- Oberdörster, G., Sharp, Z., Atudorei, V., Elder, A., Gelein, R., Kreyling, W., Cox, C. (2004). Translocation of inhaled ultrafine particles to the brain. *Inhalation Toxicol.* 16, 437–445. <https://doi.org/10.1080/08958370490439597>
- Olfert, J.S., Collings, N. (2005). New method for particle mass classification—the Couette centrifugal particle mass analyzer. *J. Aerosol Sci.* 36, 1338–1352. <https://doi.org/10.1016/j.jaerosci.2005.03.006>
- Onasch, T.B., Trimborn, A., Fortner, E.C., Jayne, J.T., Kok, G.L., Williams, L.R., Davidovits, P., Worsnop, D.R. (2012). Soot particle aerosol mass spectrometer: development, validation, and initial application. *Aerosol Sci. Technol.* 46, 804–817. <https://doi.org/10.1080/02786826.2012.663948>
- Prather, K.A., Nordmeyer, T., Salt, K. (1994). Real-time characterization of individual aerosol particles using time-of-flight mass spectrometry. *Anal. Chem.* 66, 1403–1407. <https://doi.org/10.1021/ac00081a007>
- Ristimäki, J. (2006). Sampling and measurement methods for diesel exhaust aerosol. Doctoral dissertation. Tampere University. <http://urn.fi/URN:NBN:fi:tty-200810021102>
- Saarikoski, S., Williams, L.R., Spielman, S.R., Lewis, G.S., Eiguren-Fernandez, A., Aurela, M., Hering, S.V., Teinilä, K., Croteau, P., Jayne, J.T., Hohaus, T., Worsnop, D.R., Timonen, H. (2019). Laboratory and field evaluation of the Aerosol Dynamics Inc. concentrator (ADIC) for aerosol mass spectrometry. *Atmos. Meas. Tech.* 12, 3907–3920. <https://doi.org/10.5194/amt-12-3907-2019>



- Scheibel, H.G., Porstendörfer, J. (1983). Generation of monodisperse Ag- and NaCl-aerosols with particle diameters between 2 and 300 nm. *J. Aerosol Sci.* 14, 113–126. [https://doi.org/10.1016/0021-8502\(83\)90035-6](https://doi.org/10.1016/0021-8502(83)90035-6)
- Skillas, G., Künzel, S., Burtscher, H., Baltensperger, U., Siegmann, K. (1998). High fractal-like dimension of diesel soot agglomerates. *J. Aerosol Sci.* 29, 411–419. [https://doi.org/10.1016/S0021-8502\(97\)00448-5](https://doi.org/10.1016/S0021-8502(97)00448-5)
- Willis, M.D., Lee, A.K.Y., Onasch, T.B., Fortner, E.C., Williams, L.R., Lambe, A.T., Worsnop, D.R., Abbatt, J.P.D. (2014). Collection efficiency of the soot-particle aerosol mass spectrometer (SP-AMS) for internally mixed particulate black carbon. *Atmos. Meas. Tech.* 7, 4507–4516. <https://doi.org/10.5194/amt-7-4507-2014>
- Zelenyuk, A., Imre, D. (2005). Single particle laser ablation time-of-flight mass spectrometer: An introduction to SPLAT. *Aerosol Sci. Technol.* 39, 554–568. <https://doi.org/10.1080/027868291009242>